The Effect of Bubble Acceleration on the Liquid Film Thickness in Micro Tubes

Youngbae Han and Naoki Shikazono

Department of Mechanical Engineering, The University of Tokyo
Hongo 7-3-1, Bunkyo-ku, Tokyo, 113-8656, Japan
Tel: +81-3-5841-6419; Fax: +81-3-5800-6999

Email address: ybhan@feslab.t.u-tokyo.ac.jp (Youngbae Han),
shika@feslab.t.u-tokyo.ac.jp (Naoki Shikazono).

Abstract

Liquid film thickness is an important parameter for predicting boiling heat transfer in micro tubes. In the previous study (Han and Shikazono, 2009a), liquid film thickness under the steady condition was investigated and an empirical correlation for the initial liquid film thickness based on capillary number, Reynolds number and Weber number was proposed. However, under flow boiling conditions, bubble velocity is not constant but accelerated due to evaporation. It is necessary to consider this bubble acceleration effect on the liquid film thickness, since it affects viscous, surface tension and inertia forces in the momentum equation. In addition, viscous boundary layer develops, and it may also affect the liquid film thickness. In the present study, the effect of bubble acceleration is investigated. Laser focus displacement meter is used to measure the liquid film thickness. Ethanol, water and FC-40 are used as working fluids. Circular tubes with three different inner diameters, D = 0.5, 0.7 and 1.0 mm, are used. The increase of liquid film thickness with capillary number is restricted by the bubble acceleration. Finally, an empirical correlation is proposed for the liquid film thickness of accelerated flows in terms of capillary number and Bond number based on the bubble acceleration.

NOMENCLATURE

a	bubble acceleration, [m/s^2]
Bo	Bond number based on the bubble acceleration, $Bo = \rho a D^2/\sigma$
Ca	capillary number, $Ca = \mu U/\sigma$
D	tube inner diameter, [m]
Z	axial distance from the initial gas-liquid interface, [m]
n	refractive index
R	tube radius, [m]
Re	Reynolds number, $Re = \rho UD/\mu$
t	time, [s]
U	bubble velocity, [m/s]
We	Weber number, $We = \rho U^2 D/\sigma$

Greek Symbols

δ	liquid film thickness, [m]
δ^*	viscous boundary layer thickness, [m]
λ	transition region length, [m]
μ	viscosity, [Pa·s]
ν	kinematic viscosity, [m^2/s]
ρ	density, [kg/m^3]
σ	surface tension, [N/m]

Subscripts

0	initial
1	through Z axis in Fig. 5
2	through X axis in Fig. 5
accel	accelerated condition
steady	steady condition

1. INTRODUCTION

Slug flow in micro tubes is encountered in many industrial appliances, e.g., micro heat exchanger, micro reactor, coating process, oil recovery etc. In slug flow, sequential bubbles confined by liquid slugs flow with the liquid film formed between the tube wall and the bubble. Slug flow is characterized by the enhanced mixing due to the circulation in liquid slug and the superior heat and mass transfer through the thin liquid film (Taha and Cui, 2006). Evaporation heat transfer coefficient through thin liquid film is modeled as follows:

$$h = \frac{k}{\delta}, \tag{1}$$

where h is the heat transfer coefficient, k is thermal conductivity of the liquid and δ is the liquid film thickness. Thus, liquid film thickness is one of the key parameters for predicting flow boiling heat transfer coefficient in micro tubes (Thome et al., 2004; Kenning et al., 2006; Qu and Mudawar, 2003; Saitoh et al., 2007). It is crucial to collect accurate liquid film thickness data for developing precise heat transfer models.

Several experimental methods have been used to measure the liquid film thickness in micro tubes. Liquid film thickness can be measured from the difference between bubble velocity and mean velocity, assuming that liquid film is stationary. Taylor (1961) measured the thickness of liquid film deposited on the wall with such a method in wide range of capillary number. It was found that the ratio of the bubble velocity to mean velocity approaches an asymptotic value, 0.55. This asymptotic value was reported as 0.60 by the experimental research of Cox (1962). Schwartz et al. (1986) used the same method as Taylor (1961) to investigate the effect of finite bubble length on the liquid film thickness. It was reported that the long bubbles move faster than the short ones. Aussillous and Quere (2000) measured the liquid film thickness using fluids with relatively low surface tension. It was found that the liquid film thickness deviates from the Taylor's data at relatively high capillary numbers. Visco-inertia regime where the effect of inertia force on the liquid film thickness becomes significant was demonstrated. The converging trend of the liquid film thickness with capillary number

and the deviation from the Taylor's data due to the inertial effect were explained with a simple scaling analysis. It was also observed that the liquid film thickness is determined by the viscous boundary layer when viscous boundary layer is thin.

Liquid film thickness can be measured from the temperature change of the channel wall under the assumption that the whole liquid film on the wall evaporates and the heat is consumed by the evaporation of the liquid film. Cooper (1969) measured the liquid film thickness and investigated the bubble growth in nucleate pool boiling. Moriyama and Inoue (1996) measured the thickness of the liquid film formed by a vapor bubble expansion in a narrow gap. It was reported that when acceleration becomes large, liquid film thickness is affected by the viscous boundary layer. Their experimental data was correlated in terms of dimensionless boundary layer thickness, capillary number and Bond number.

Several optical methods have been applied for the liquid film thickness measurement, e.g. optical interface detection, laser extinction, total light reflection, laser focus displacement etc. Ursenbacher et al. (2004) developed a new optical method to detect the instantaneous vapor-liquid interface. Interface of stratified two-phase flow in a 13.6 mm inner diameter tube was detected in their experiment. Utaka et al. (2007) measured the liquid film thickness formed by a vapor bubble in a narrow gap mini-channel with laser extinction method. Liquid film thickness from 2 μm to 30 μm was measured in 0.5, 0.3 and 0.15 mm gap channels. It was concluded that the boiling phenomena were determined by two characteristic periods, i.e. the micro-layer dominant and the liquid saturated periods. Hurlburt and Newell (1996) developed a device which measures the liquid film thickness from the total reflection of light. Using the same method, Shedd and Newell (2004) measured the liquid film thickness of the air/water two-phase flow in round, square and triangular tubes. Han and Shikazono (2009a, b) measured the liquid film thickness under adiabatic condition with laser focus displacement meter. The effect of inertia force on the liquid film thickness was investigated using micro circular tubes and square channels with different hydraulic diameters and several working fluids. Empirical correlations based on capillary number, Reynolds number and Weber number were proposed. Other measurement methods, e.g. acoustical methods, electrical

methods and nucleonic methods are summarized well in the review paper of Ribatski and Tibirica (2008).

Although many methods have been applied to measure the liquid film thickness, researches on measuring liquid film thickness in micro tubes are still limited. Besides, most of the experiments in micro tubes were conducted under steady condition. However, under flow boiling conditions, the bubble velocity is not constant but accelerated, and it is necessary to consider this acceleration effect on the liquid film thickness (Kenning, et al., 2006). Acceleration may affect the balance between viscous, surface tension and inertia forces in the momentum equation. In addition, viscous boundary layer develops, and it may also affect the liquid film thickness. In the present study, the effect of bubble acceleration on the liquid film thickness is investigated experimentally.

2. EXPERIMENTAL SETUP AND PROCEDURES

2.1 Experimental setup

Circular tubes made of Pyrex glass with D = 0.5, 0.7 and 1.0 mm were used as test tubes. Tube diameter was measured with a microscope and the averaged value of the inlet and outlet inner diameters was used for the experimental data reduction. Table 1 shows the dimensions of the micro tubes. The differences of inlet and outlet diameters were less than 1% for all tubes. Tube lengths are 250 mm for all tubes. Air was used as the gas phase. Ethanol, water and FC-40 were used as the working fluids in order to investigate the Reynolds number dependence. Reynolds number of ethanol is about 6 times larger than that of FC-40, and Reynolds number of water is again about 6 times larger than that of ethanol at the same capillary number (see Fig.8 in Han and Shikazono, 2009a).

Figure 1 shows the schematic diagram of the experimental setup. One end of Pyrex glass tube is connected to the syringe and the other end is opened to the air. Actuator motor (EZHC6A-101, Oriental motor) is used to pull the liquid in the micro tube. The velocity of the actuator motor ranges from 0 to 0.2 m/s. Syringes with several cross

sectional areas are used to control the liquid velocity in the test section. Thus, the range of bubble velocity in the present experiment is varied from 0 to 7 m/s. The bubble velocity and acceleration are calculated from the images obtained by the high-speed camera. In the present experiment, gas inlet is open to the atmosphere and the pressure in the test tube is almost 1 atm. Thus, present result is only applicable to low pressure conditions at which the effect of density and viscosity of gas phase are negligible.

Laser focus displacement meter (hereafter LFDM; LT9010M, Keyence) is used to measure the liquid film thickness. LFDM has been used by several researchers for the measurement of the liquid film thickness (Takamasa and Kobayashi, 2000; Hazuku et al., 2005; Han and Shikazono, 2009a, b). It is reported that LFDM can measure the liquid film thickness very accurately within 1% error (Hazuku et al., 2005). Detailed measurement uncertainties are presented in our previous paper (Han and Shikazono, 2009a). Figure 2 shows the principle of the LFDM. The position of the target surface can be determined by the displacement of objective lens moved by the tuning fork. The intensity of the reflected light becomes highest in the light-receiving element when the focus is obtained on the target surface. Objective lens is vibrated continually in the range of ±0.3 mm. Relative distances between interfaces can be detected during one cycle of the objective lens vibration. The resolution of the present laser focus displacement meter is 0.01 μm, the laser spot diameter is 2 μm and the response time is 640 μs. Thus, it is possible to measure the liquid film thickness instantaneously and locally. Measured liquid film thickness is transformed to DC voltage signal in the range of ±10V. Output signal was sent to PC through GPIB interface and recorded with LabVIEW.

2.2 Correction for the tube wall curvature

As the laser beam passes through the tube wall, focus is scattered within a certain range due to the difference of curvatures between the axial and azimuthal directions. Cover glass and glycerol were used to remove the curvature effect caused by the outer wall as shown in Fig. 3. Refractive index of glycerol (n = 1.47) is almost the same with that of the Pyrex glass (n = 1.474), thus the refraction of laser between glycerol and Pyrex glass can be neglected. Refractive indices of ethanol, water and FC-40 are 1.36, 1.33 and

1.29. It is difficult to detect the interface between inner wall and liquid, because the difference of the refractive indices of the wall and the liquid is small. Therefore, the distance from the cover glass to the dry inner wall is initially measured without flowing the liquid. Then, the thickness with liquid film is measured. The liquid film thickness is calculated from the difference of these two values.

The effect of the inner wall curvature is corrected by the equation suggested by Takamasa and Kobayashi (2000). Schematic diagram of the focus scattering caused by the inner wall curvature in liquid film is shown in Fig. 4. Laser focus is scattered from δ_1 to δ_2. The intensity of the reflected light becomes highest at the center of δ_1 and δ_2. Therefore, liquid film thickness δ can be obtained as follows:

$$\delta = \frac{\delta_1 + \delta_2}{2}. \tag{2}$$

The curvature effect caused by the inner wall is small when the liquid film is thin. The scattering length (δ_2-δ_1) is less than 2% of the liquid film thickness in the present study. Refer to Han and Shikazono (2009a) for the details.

2.3 Experimental procedures

In order to investigate the effect of bubble acceleration on the liquid film thickness, measurement points are positioned at Z = 5, 10 and 20 mm away from the initial air-liquid interface position Z = 0 mm as shown in Fig. 5. For the convenience in conducting experiments, the position of LFDM is fixed by XYZ stage initially with high-speed camera and illumination equipment. Air-liquid interface is moved to the initial position, Z = 0 mm with the actuator motor to fit the distance between the initial position and the measurement position. The distance is obtained from the image captured by high-speed camera.

Figure 6 shows bubble velocity at downstream positions. Figure 7 shows the time variation of liquid film thickness at Z = 20 mm. Liquid film thickness is measured at the tube side under the condition of room temperature and 1 atm. After the initial quick

decrease, liquid film thickness decreases gradually with time. The initial quick decrease is the transition region between the bubble nose and the flat film region. If the angle of air-liquid interface is larger than about 11°, interface cannot be detected by LFDM. Thus, the whole shape of bubble nose cannot be measured and the liquid film thickness only in the transition region and the flat film region can be measured.

After the liquid film is formed, liquid film is driven by the gas flow. For constant bubble velocity experiments, liquid film is deposited on the tube wall as a constant thickness. Therefore, although liquid film is driven by gas flow, liquid film thickness at the fixed measurement position does not change and shows almost constant value. However, when the flow is accelerated, bubble velocity increases along the flow direction. Liquid film thickness is deposited thicker as bubble velocity increases along the flow direction. Liquid film thickness at the initial position is zero and liquid film is deposited with a gradient to the measurement position. In the present experiment, liquid film thickness is measured at the fixed position. This is the reason why the liquid film thickness under accelerated condition decreases gradually after the initial quick decrease. Liquid film thickness after the initial quick decrease is defined as the initial liquid film thickness as shown in Fig. 7 and this initial liquid film thickness is used for the experimental data reduction.

2.4 Definition of acceleration

In the present experiment, ethanol, water and FC-40 are used as working fluids. The bubble acceleration is simply expressed assuming that the acceleration is uniform when the flow is accelerated to a certain velocity as follows:

$$a = \frac{U^2}{2Z}, \tag{3}$$

where U is the bubble velocity at the measurement position. Figure 8 shows the bubble acceleration against capillary number under the condition of 23°C and 1 atm corresponding to the working fluids and the distances between the initial position and the measurement position. Bubble velocity at the measurement position is used for capillary number. In the present experiment, distance from the initial interface position

to the measurement position is fixed, thus the acceleration becomes larger at larger capillary numbers. At the same capillary number, as the distance Z increases, bubble acceleration decreases. Surface tension of water is quite larger than that of ethanol or FC-40 and thus bubble velocity is much higher at the same capillary number. Bubble velocities of water, ethanol and FC-40 at Ca = 0.1 are 7.77, 1.99 and 0.27 m/s, respectively. Therefore, bubble acceleration of water is much larger than that of ethanol or FC-40 at the same capillary number.

3. RESULTS AND DISCUSSION

3.1 Ethanol/air experiment

Figures 9 (a)-(c) show the dimensionless liquid film thickness against capillary number for the ethanol/air experiment. In Figs. 9 (a)-(c), liquid film thickness under accelerated condition can be divided into two regions. At small capillary numbers, liquid film thickness is identical to the data under steady condition. As capillary number increases, liquid film thickness deviates from the data under steady condition and liquid film thickness is much smaller. The experimental data obtained in previous research (Han and Shikazono, 2009a) are used for the liquid film thickness under steady condition. Empirical correlation of the initial liquid film thickness under steady condition was proposed as follows:

$$\left(\frac{\delta_0}{D}\right)_{\text{steady}} = \begin{cases} \dfrac{0.670Ca^{2/3}}{1+3.13Ca^{2/3}+0.504Ca^{0.672}Re^{0.589}-0.352We^{0.629}} & (Re<2000) \quad (4-1) \\ \dfrac{106.0\left(\mu^2/\rho\sigma D\right)^{2/3}}{1+497.0\left(\mu^2/\rho\sigma D\right)^{2/3}+7330\left(\mu^2/\rho\sigma D\right)^{2/3}-5000\left(\mu^2/\rho\sigma D\right)^{2/3}} & (Re\geq 2000) \quad (4-2) \end{cases}$$

Liquid film thickness remains constant for $Re \geq 2000$ due to the flow transition from laminar to turbulent.

In Figs. 9 (a)-(c), liquid film thicknesses under accelerated conditions are much smaller than the data under steady condition. At the same capillary number, liquid film becomes thicker along the flow direction. And for D = 0.7 and 1.0 mm tubes, liquid film

thickness shows slight decrease with capillary number. It is considered that viscous boundary layer affects the liquid film thickness. It is reported in previous researches (Moriyama and Inoue, 1996; Aussillous and Quere, 2000) that the liquid film generation is restricted by the viscous boundary layer when viscous boundary layer is thin. Viscous boundary layer thickness δ^* can be scaled as follows:

$$\delta^* \sim \left(\frac{\nu Z}{U}\right)^{1/2}, \tag{5}$$

where ν is kinematic viscosity. Even though viscous boundary layer thickness is independent of tube diameter as shown in Eq. (5), absolute liquid film thickness increases with tube diameter in the present experiment. It is considered that the liquid film thickness is not affected only by viscous boundary layer but also by surface tension. As tube diameter increases, surface tension force becomes weak and liquid film thickness increases.

When the viscous boundary layer is thick, liquid film thickness is identical to the steady condition data. On the other hand, when the viscous boundary layer is thin due to the large acceleration effect, force balance is affected by viscous boundary layer thickness and surface tension, making liquid film thickness deviate from the steady condition data.

3.2 Water/air experiment

Figures 10 (a)-(c) show the dimensionless liquid film thickness against capillary number for the water/air experiment. As in the case of ethanol/air experiment, liquid film thickness becomes identical to the steady condition data at small capillary numbers. As capillary number increases, liquid film thickness deviates from the steady condition data. As shown in Fig. 8, acceleration of water/air experiment is larger than that of ethanol/air experiment, thus liquid film thickness deviates at lower capillary number. In the ethanol/air experiment, liquid film thickness decreases with capillary number after the deviation. However, in case of water/air experiment, liquid film thickness continues to increase with capillary number after the deviation. This trend is apparent especially in

D = 0.5 mm case. Surface tension force works most strongly in the case of water/air and tube diameter D = 0.5 mm. Therefore, this trend is attributed to the surface tension effect.

As the dimensionless number for the ratio of acceleration and surface tension, Bond number based on the bubble acceleration was introduced by Moriyama and Inoue (1996) as follows:

$$Bo = \frac{\rho D^2}{\sigma}\left(\frac{U}{t_g}\right), \tag{6}$$

where t_g is the time for the interface to reach the measurement position. In their experiment, bubble acceleration could be obtained directly from the variation of bubble velocity using captured images. However, bubble acceleration is proportional to the square of time and the calculation error can be larger. Therefore, they used (U/t_g) term for the bubble acceleration. Also in the present experiment, the bubble acceleration is not obtained directly from the variation of bubble velocity. Under the assumption of uniform acceleration, the bubble acceleration is obtained as Eq. (3). Bond number based on the bubble acceleration is introduced as follows:

$$Bo_{\mathrm{accel}} = \frac{\rho a D^2}{\sigma}, \tag{7}$$

3.3 FC-40/air experiment

Figures 11 (a)-(c) show the dimensionless liquid film thickness against capillary number for the FC-40/air experiment. Viscous boundary layer develops quickly in FC-40 due to its large viscosity. In order to obtain thinner viscous boundary layer data, measurement position is changed as Z = 2.5, 5 and 10 mm. As in the cases of ethanol/air and water/air experiments, liquid film thickness is almost identical to the steady condition data at small capillary number. As capillary number increases, liquid film thickness deviates from the steady condition data. Liquid film thickness decreases with capillary number after the deviation. This may be due to small surface tension of FC-40.

3.4 Viscous boundary layer

The effect of viscous boundary layer on the liquid film thickness is investigated. Figure 12 shows dimensionless liquid film thickness δ_0/D against dimensionless viscous boundary layer thickness δ^*/D. The definition of viscous boundary layer thickness is obtained as follows:

$$\delta^* = \left(\frac{\nu Z}{U}\right)^{1/2}, \tag{8}$$

In Fig. 12, it is shown that experimental values approach asymptotic lines when viscous boundary layer becomes thin. These lines correspond to the restriction of the liquid film thickness caused by the thin viscous boundary layer. These asymptotic lines are different for three working fluids, which implies that not only viscous boundary layer thickness but also other parameters are affecting the liquid film development. At the same viscous boundary layer thickness, asymptotic dimensionless liquid film thickness becomes thinner as surface tension increases.

3.5 Scaling analysis for the bubble acceleration

Bretherton (1961) proposed a theoretical correlation for the liquid film thickness with lubrication equations as follows:

$$\frac{\delta_0}{R} = 0.643\left(\frac{3\mu U}{\sigma}\right)^{2/3}, \tag{9}$$

where R is the tube radius. Aussillous and Quere (2000) made a scaling analysis on the liquid film thickness based on Bretherton's theoretical analysis (1961). The momentum balance and the curvature matching between the bubble nose and the transition region are expressed as follows:

$$\frac{\mu U}{\delta_0^2} \sim \frac{1}{\lambda}\left\{\frac{\sigma}{R-\delta_0}\right\}, \tag{10}$$

$$\frac{\delta_0}{\lambda^2} \sim \frac{1}{R-\delta_0}, \tag{11}$$

where λ is the transition region length as shown in Fig. 13. The relation for δ_0/D is deduced as follows:

$$\frac{\delta_0}{D} \sim \frac{Ca^{2/3}}{1+Ca^{2/3}}. \tag{12}$$

Based on Eq. (12), Taylor's experimental data was fitted as follows (Aussillous and Quere, 2000):

$$\frac{\delta_0}{D} = \frac{0.67Ca^{2/3}}{1+3.35Ca^{2/3}}. \tag{13}$$

Equation (13) is called Taylor's law.

Figure 13 shows the schematic diagram of the velocity profiles under steady and accelerated conditions. Under accelerated condition, bubble nose curvature is affected by the viscous boundary layer. This is considered to be the reason for the decrease of the liquid film thickness. Under the bubble acceleration condition, the bubble nose curvature is modified as:

$$\kappa \sim \left(\frac{1}{R-\delta_0}\right)\cdot f, \tag{14}$$

where *f* is the modification coefficient for the velocity profile change in the liquid slug under accelerated condition. If the curvature of bubble nose in the R.H.S. of Eqs. (10) and (11) is replaced by Eq. (14), Eq. (13) can be rewritten as follows:

$$\frac{\delta_0}{D} \sim \frac{0.67 Ca^{2/3} \cdot f}{1 + 3.35 Ca^{2/3} \cdot f}, \tag{15}$$

Modification coefficient f can be expressed from Eq. (15) as:

$$f \sim \frac{0.67 Ca^{2/3}}{\delta_0 / D} - 3.35 Ca^{2/3}, \tag{16}$$

As explained in section 3.2, liquid film thickness under accelerated condition is affected by the viscous boundary layer and surface tension. Bond number based on the bubble acceleration Bo_{accel} is introduced for the ratio of acceleration effect and surface tension force. It is expected that function f has a relation to Bo_{accel}. Figure 14 shows the relationship between the R.H.S. of Eq. (16) and the acceleration Bond number, Eq. (7). Only the experimental data that deviate from the steady condition data are used. As shown in Fig. 14, the change of bubble nose curvature can be scaled very well by Bond number based on the bubble acceleration. All the data in the Fig. 14 are well correlated with a single fitting line as:

$$f = 0.692 Bo_{\text{accel}}^{0.414}, \tag{17}$$

Substituting Eq. (17) in Eq. (15), a correlation for the liquid film thickness under bubble acceleration can be obtained as follows:

$$\left(\frac{\delta_0}{D}\right)_{\text{accel}} = \frac{0.968 Ca^{2/3} Bo_{\text{accel}}^{-0.414}}{1 + 4.838 Ca^{2/3} Bo_{\text{accel}}^{-0.414}}, \tag{18}$$

As shown in Figs. 9-11, liquid film thickness under accelerated condition is identical to that under steady condition when capillary number is small. Thus, in the present study, liquid film thickness in the whole capillary number range is simply expressed as follows:

$$\frac{\delta_0}{D} = min\left[\left(\frac{\delta_0}{D}\right)_{\text{steady}}, \left(\frac{\delta_0}{D}\right)_{\text{accel}}\right], \tag{19}$$

where, Eq. (4) is used for $(\delta_0/D)_{\text{steady}}$ and Eq. (18) is used for $(\delta_0/D)_{\text{accel}}$.

Moriyama and Inoue (1996) proposed an empirical correlation for the liquid film thickness including the acceleration effect as follows:

$$\frac{\delta}{D} = \begin{cases} 0.10\left(\delta^*\right)^{0.84} & (Bo > 2) \\ 0.07\,Ca^{0.41} & (Bo \le 2) \end{cases}, \tag{20}$$

$$\delta^* = \frac{\sqrt{\nu t_g}}{D}, \tag{21}$$

where δ^* is the dimensionless viscous boundary layer thickness and t_g is the time for the interface to reach the measurement position. Assuming uniform acceleration, t_g in Eq. (21) can be expressed as:

$$t_g = \frac{Z}{2U}. \tag{22}$$

As shown Fig. 15, Eq. (20) underpredicts the present experimental data. This trend was also reported in other experimental research (Kenning et al., 2006). If Eq. (20) is multiplied by 3.5, the agreement with the present experimental data becomes much better. However, prediction shows different trends for three working fluids. Boundary layer thickness cannot express the effect of physical property difference. Fig. 16 shows the comparison between present correlation Eq. (19) and the experimental data. Present correlation can predict the liquid film thickness more accurately within the range of ±15 % accuracy. Figs. 17 (a)-(c) show the comparison between the experimental data against capillary number. Equation (19) can predict liquid film thickness very accurately for three different working fluids.

4. CONCLUSIONS

The effect of bubble acceleration on the liquid film thickness in micro tubes was investigated. When the bubble is accelerated, viscous boundary layer strongly affects the liquid film thickness. If the viscous boundary layer is thick, liquid film thickness can be determined by the steady condition prediction. However, if the viscous boundary layer is thin, liquid film thickness becomes thinner due to the acceleration effect. Experimental correlation for the liquid film thickness under bubble acceleration is proposed in terms of capillary number and Bond number. The present correlation can predict liquid film thickness within the range of ±15 % accuracy. In order to develop precise flow boiling models in a micro tube, it is necessary to consider the effect of bubble acceleration on the liquid film thickness.

ACKNOWLEDGEMENT

We would like to thank Prof. Kasagi, Prof. Suzuki and Dr. Hasegawa for the fruitful discussions and suggestions. This work is supported through Grant in Aid for Scientific Research (No. 20560179) by MEXT, Japan.

REFERENCES

Aussillous, P., Quere, D., 2000. Quick deposition of a fluid on the wall of a tube. Phys. Fluids 12, 2367-2371.

Bretherton, F. P., 1961. The motion of long bubbles in tubes. J. Fluid Mech. 10, 166-188.

Cooper, M. G., 1969. The microlayer and bubble growth in nucleate pool boiling. Int. J. Heat Mass Transfer 12, 915-933.

Cox, B. G., 1964. An experimental investigation of the streamlines in viscous fluid expelled from a tube. J. Fluid Mech. 20, 193-200.

Han, Y., Shikazono N., 2009a. Measurement of the liquid film thickness in micro tube slug flow. Int. J. Heat Fluid Flow 35, 896-903.

Han, Y., Shikazono N., 2009b. Measurement of Liquid Film Thickness in Micro Square Channel. submitted to Int. J. Multiphase Flow, 30, 842-853.

Hazuku, T., Fukamachi, N., Takamasa, T., Hibiki, T., Ishii, M., 2005. Measurement of liquid film in microchannels using a laser focus displacement meter. Exp. Fluids 38, 780-788.

Hurlburt, E. T., Newell, T. A., 1996. Optical measurement of liquid film thickness and wave velocity in liquid film flows. Exp. Fluids 21, 357-362.

Kenning, D. B. R., Wen, D. S., Das, K. S., Wilson, S. K., 2006. Confined growth of a vapour bubble in a capillary tube at initially uniform superheat: Experiments and modeling. Int. J. Heat Mass Transfer 49, 4653-4671.

Moriyama, K., Inoue, A., 1996. Thickness of the liquid film formed by a growing bubble in a narrow gap between two horizontal plates. Trans. of the ASME 118, 132-139.

Qu, W., Mudawar, I., 2004. Flow boiling heat transfer in two-phase micro-channel heat sink-II. Annular two-phase flow model. Int. J. Heat Mass Transfer 46, 3387-3401.

Ribatski, G., Tibirica, C. B., 2008. Film thickness measurement techniques applied to microscale two-phase flow systems. ECI International Conference on Heat Transfer and Fluid Flow in Microscale, Whistler, Canada.

Saitoh, S., Daiguji, H., Hihara, H., 2007. Correlation for boiling heat transfer of R-134a in horizontal tubes including effect of tube diameter. Int. J. Heat Mass Transfer 50, 5215-5225.

Shedd, T. A., Newell, T. A., 2004. Characteristics of the liquid film and pressure drop in horizontal, annular, two-phase flow through round, square and triangular tubes. J. Fluid Eng. 126, 807-817.

Taha, T., Cui, Z. F., 2006. CFD modelling of slug flow inside square capillaries, Chem. Eng. Sci. 61, 665-675.

Takamasa, T., Kobayashi, K., 2000. Measuring interfacial waves on film flowing down tube inner wall using laser focus displacement meter. J. Multiphase Flow 26, 1493-1507.

Taylor, G. I., 1961. Deposition of a viscous fluid on the wall of a tube. J. Fluid Mech. 10, 161-165.

Thome, J. R., Dupont, V., Jacobi, A. M., 2004. Heat transfer model for evaporation in micro channels. Part I: presentation of the model. Int. J. Heat Mass Transfer 47, 3375-3385.

Ursenbacher, T., Wojtan, L., Thome, J. R., 2004. Interfacial measurements in stratified types of flow. Part I: New optical measurement technique and dry angle measurements. Int. J. Multiphase Flow 30, 107-124.

Utaka, Y., Okuda, S., Tasaki, Y., 2007. Structure of micro-layer and characteristics of boiling heat transfer in narrow gap mini-channel system. Trans. of the JSME Series B 73, 1929-1935.

Table 1 Dimensions of the micro tubes.

Circular tube		
I.D. (mm)	O.D. (mm)	Length (mm)
0.995	1.6	250
0.715	1.0	250
0.487	0.8	250

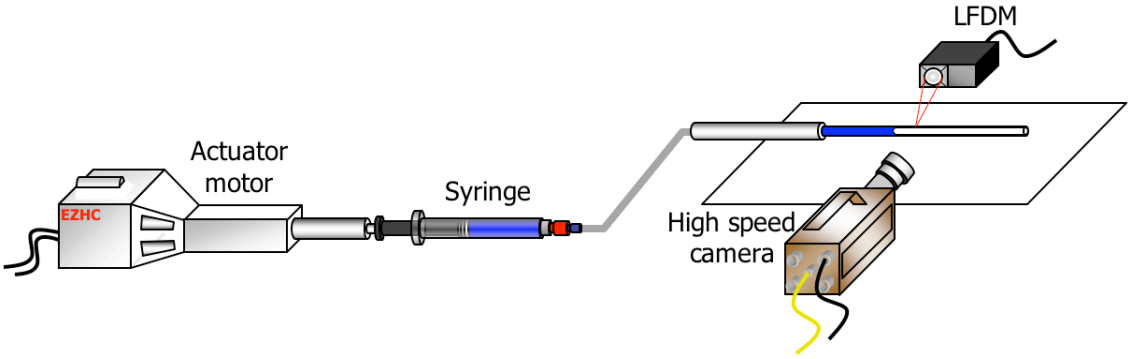

Fig. 1 Schematic diagram of the experimental setup.

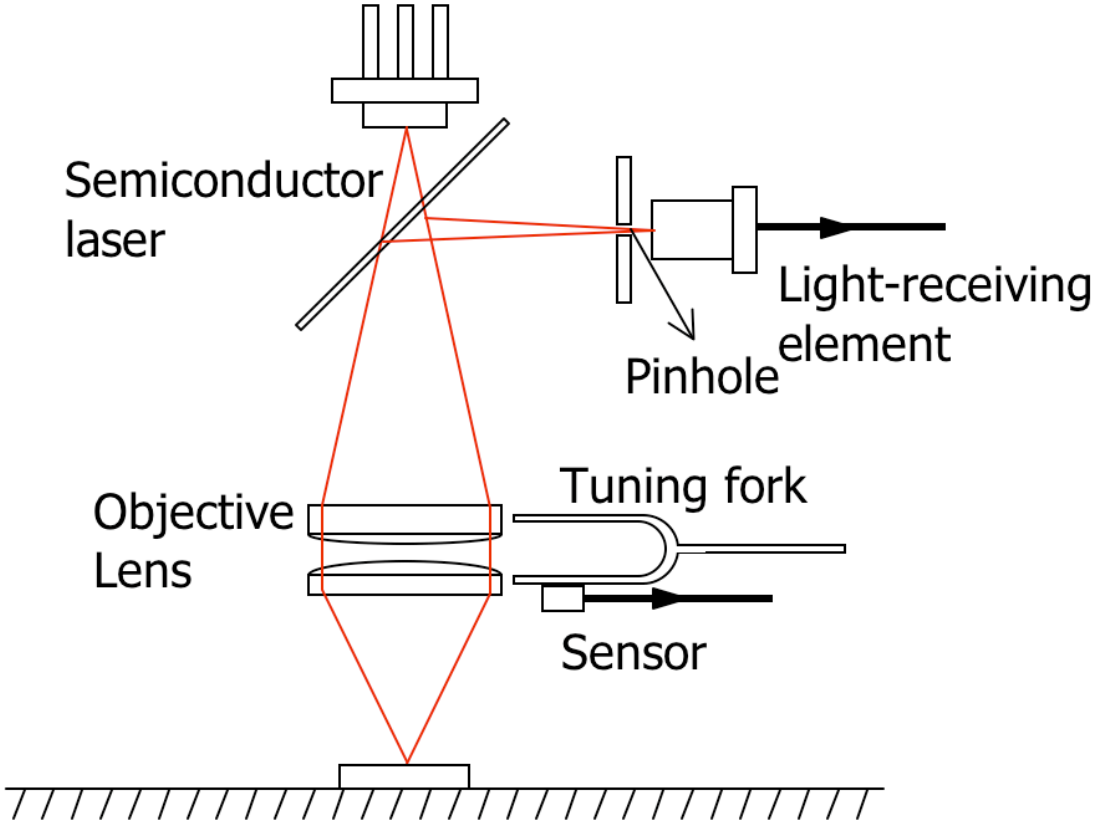

Fig. 2 Principle of laser focus displacement meter.

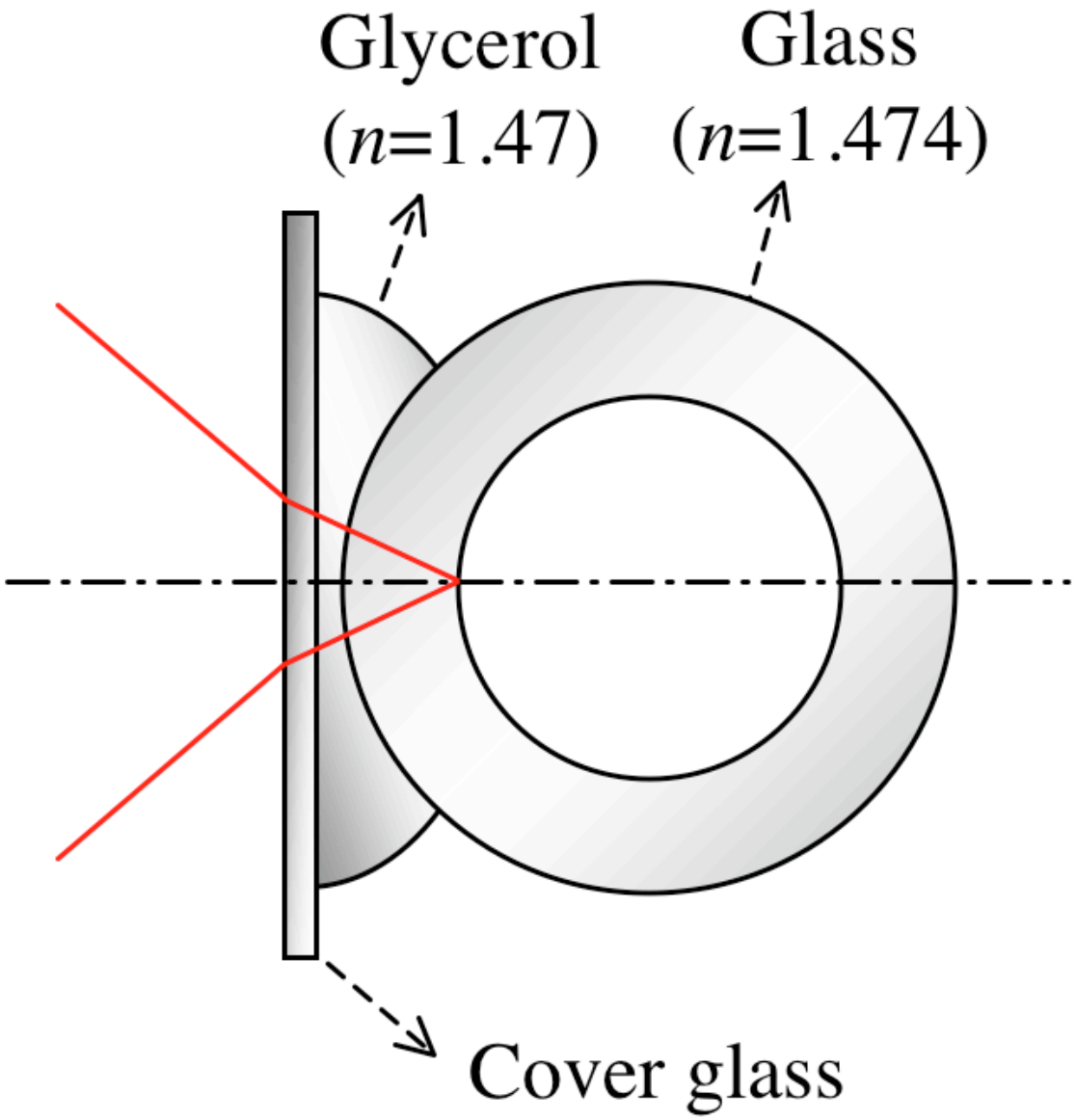

Fig. 3 Correction for the outer wall curvature.

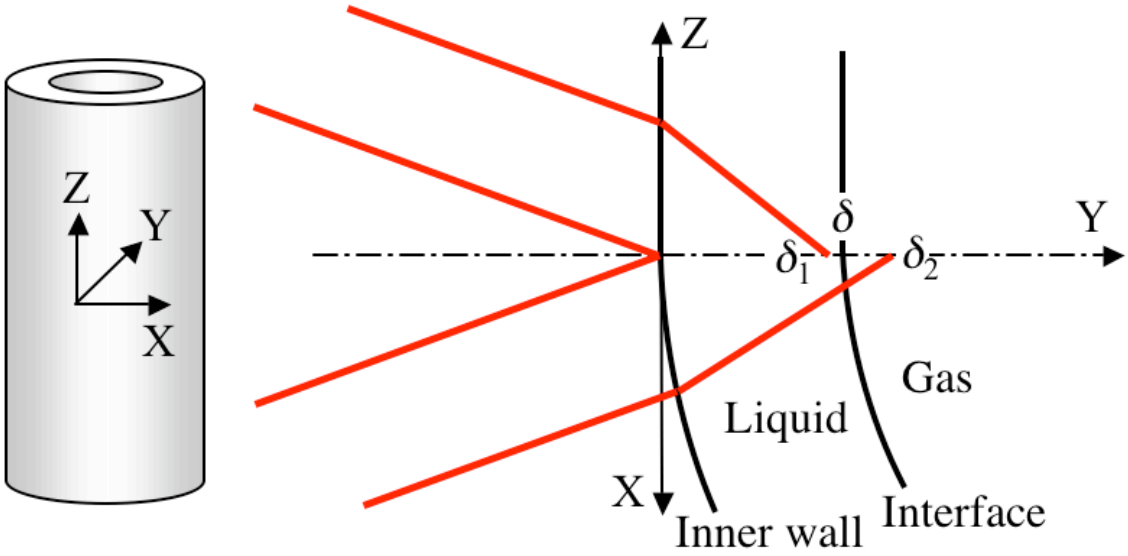

Fig. 4 Focus scattering caused by inner wall curvature.

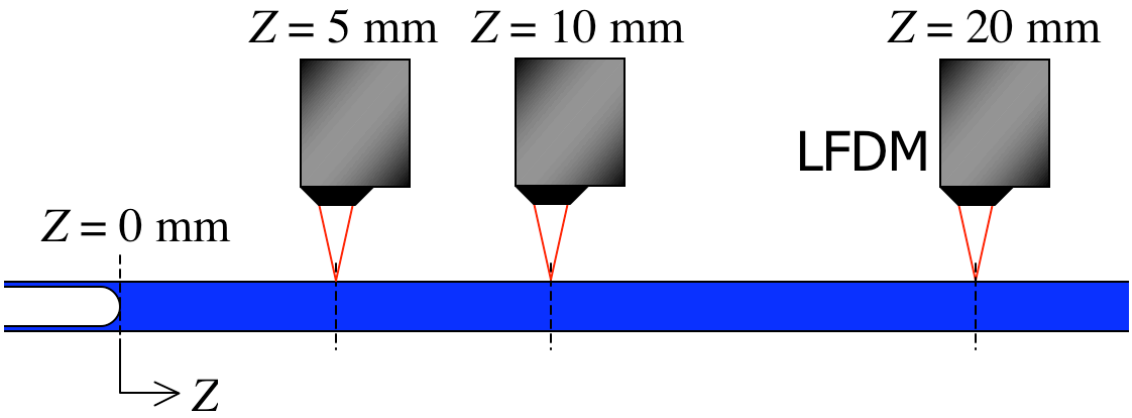

Fig. 5 Initial bubble location $Z = 0$ mm and the measuring points, $Z = 5$, 10 and 20 mm.

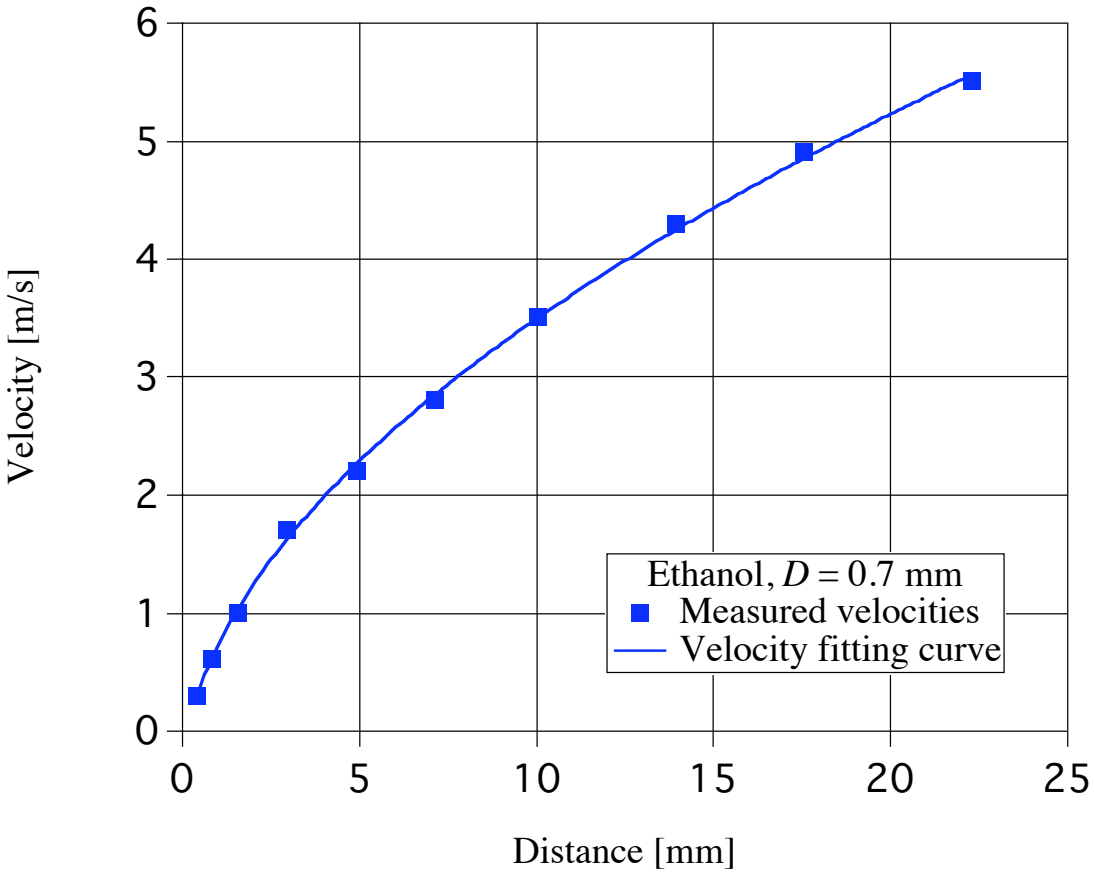

Fig. 6 Measured bubble velocity at downstream positions.

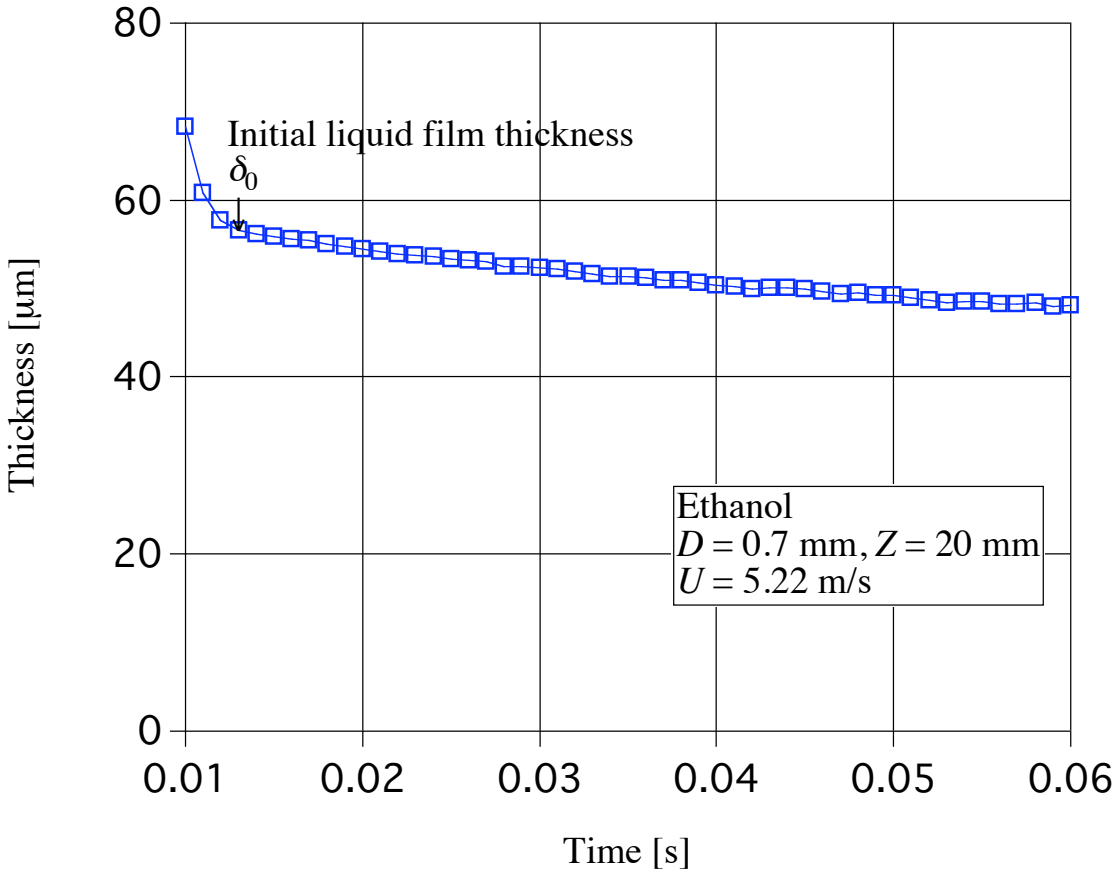

Fig. 7 Liquid film thickness against time, ethanol, D = 0.7 mm, Z = 20 mm, U = 5.22 m/s.

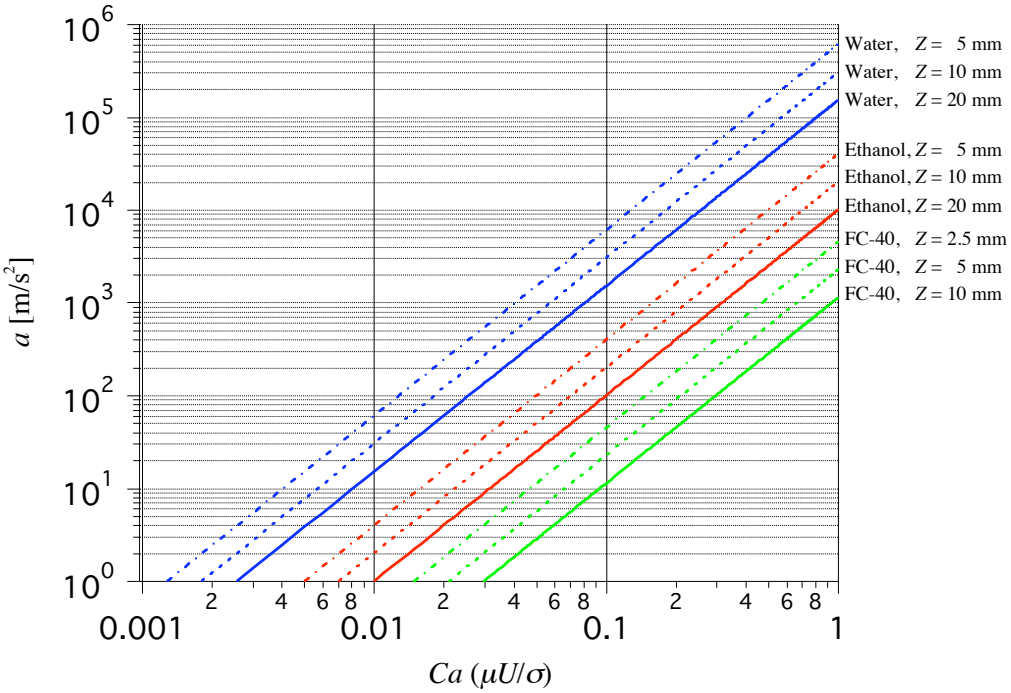

Fig. 8 Bubble acceleration ($a = U^2/2Z$) against capillary number ($Ca = \mu U/\sigma$) under the condition of 23°C and 1 atm.

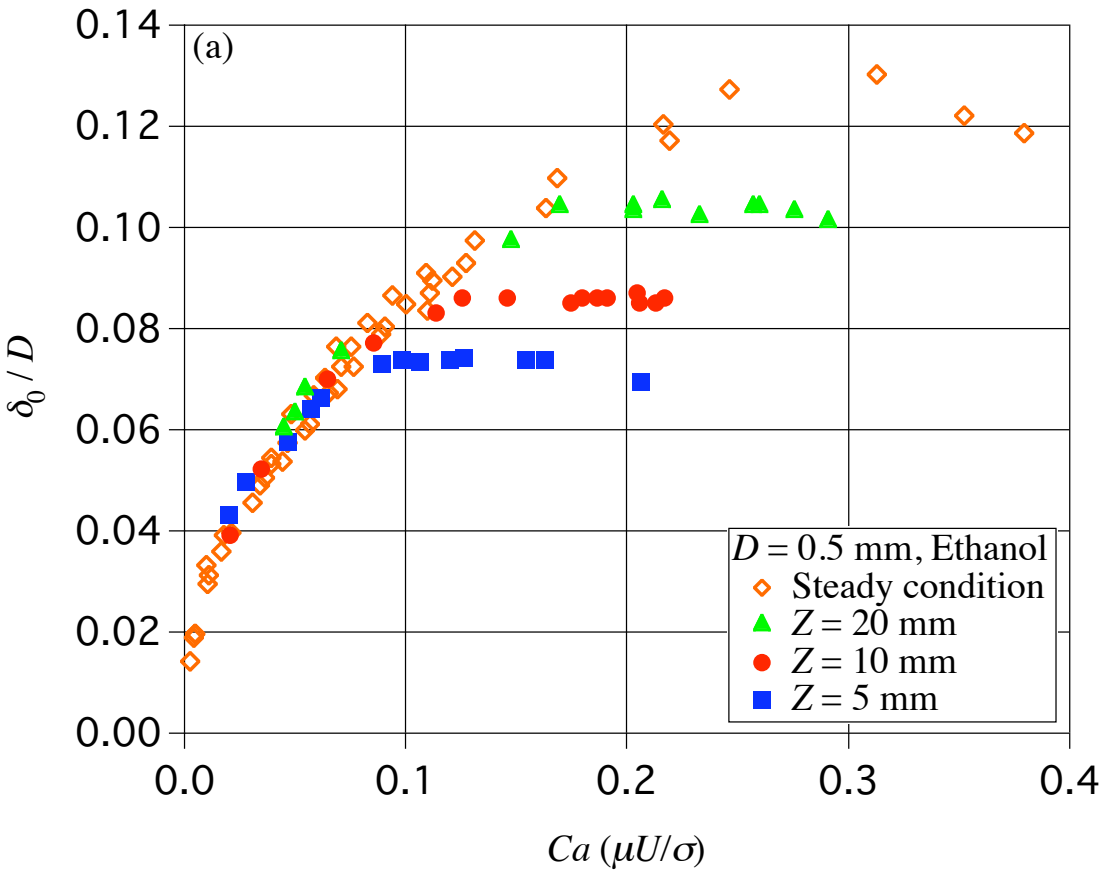
(a)
0.14
0.12
0.10
0.08
0.06
0.04
0.02
0.00
0.0
0.1
0.2
0.3
0.4
δ_0 / D
Ca ($\mu U/\sigma$)
D = 0.5 mm, Ethanol
Steady condition
Z = 20 mm
Z = 10 mm
Z = 5 mm

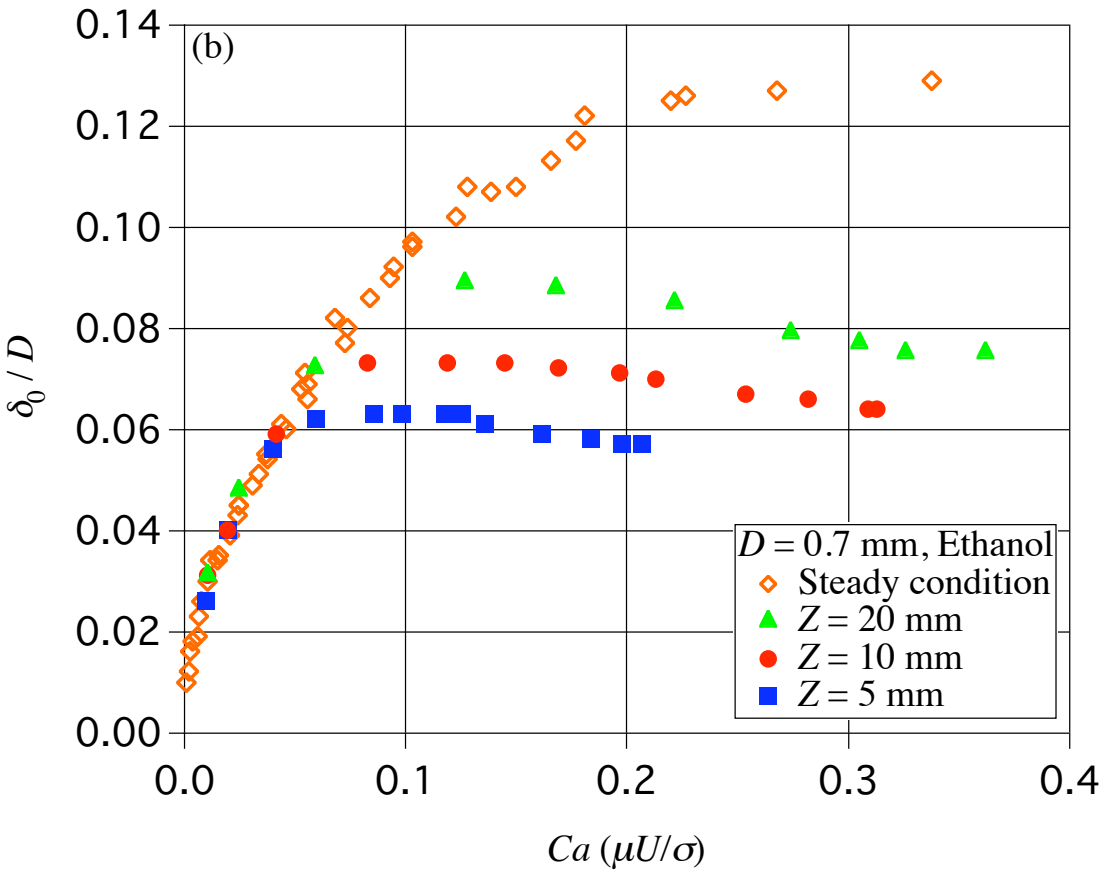
(b)
0.14
0.12
0.10
0.08
0.06
0.04
0.02
0.00
0.0
0.1
0.2
0.3
0.4
δ_0 / D
Ca ($\mu U/\sigma$)
D = 0.7 mm, Ethanol
Steady condition
Z = 20 mm
Z = 10 mm
Z = 5 mm

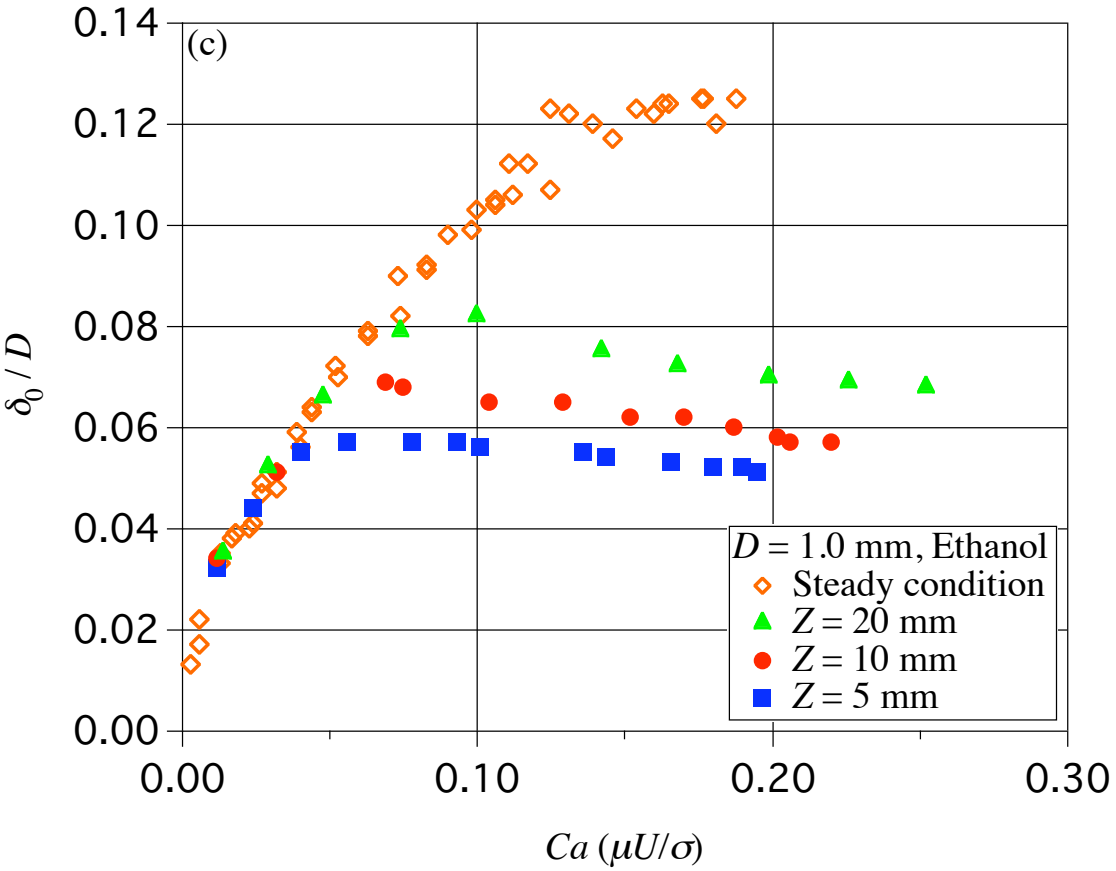

Fig. 9 Dimensionless liquid film thickness (δ_0/D) against capillary number ($Ca = \mu U/\sigma$) at different measuring points for the ethanol/air experiment, Z = 5, 10 and 20 mm, (a) D = 0.5 mm, (b) D = 0.7 mm, (c) D = 1.0 mm.

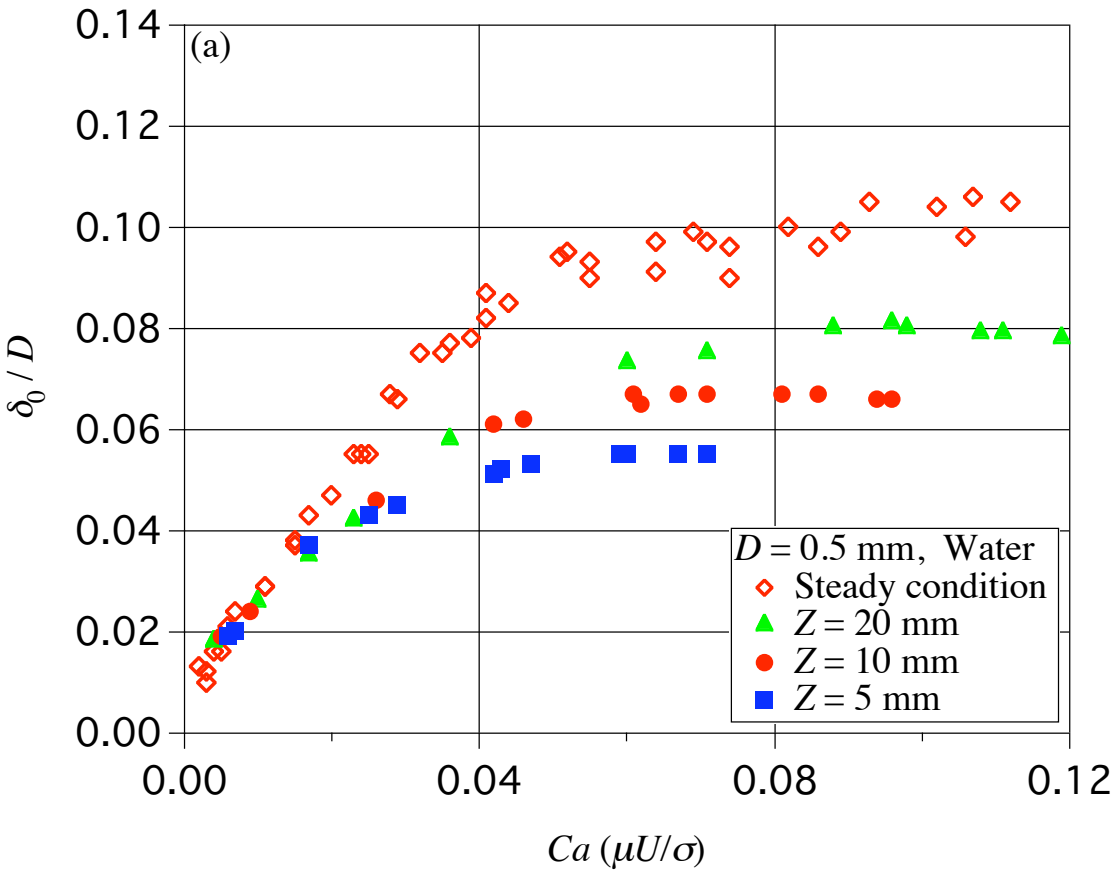
(a)
0.14
0.12
0.10
0.08
0.06
0.04
0.02
0.00
0.00
0.04
0.08
0.12
δ_0 / D
$Ca\ (\mu U/\sigma)$
$D = 0.5$ mm, Water
Steady condition
$Z = 20$ mm
$Z = 10$ mm
$Z = 5$ mm

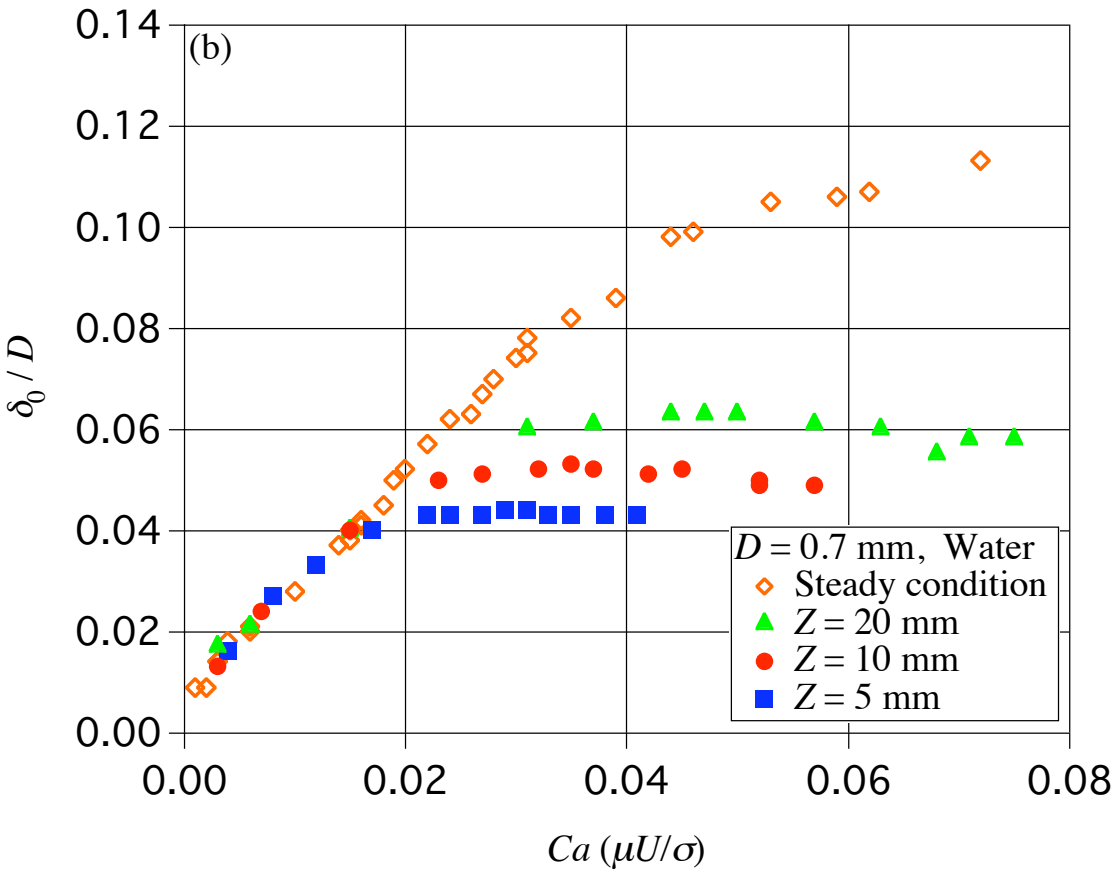
(b)
0.14
0.12
0.10
0.08
0.06
0.04
0.02
0.00
0.00
0.02
0.04
0.06
0.08
δ_0 / D
$Ca\ (\mu U/\sigma)$
$D = 0.7$ mm, Water
Steady condition
$Z = 20$ mm
$Z = 10$ mm
$Z = 5$ mm

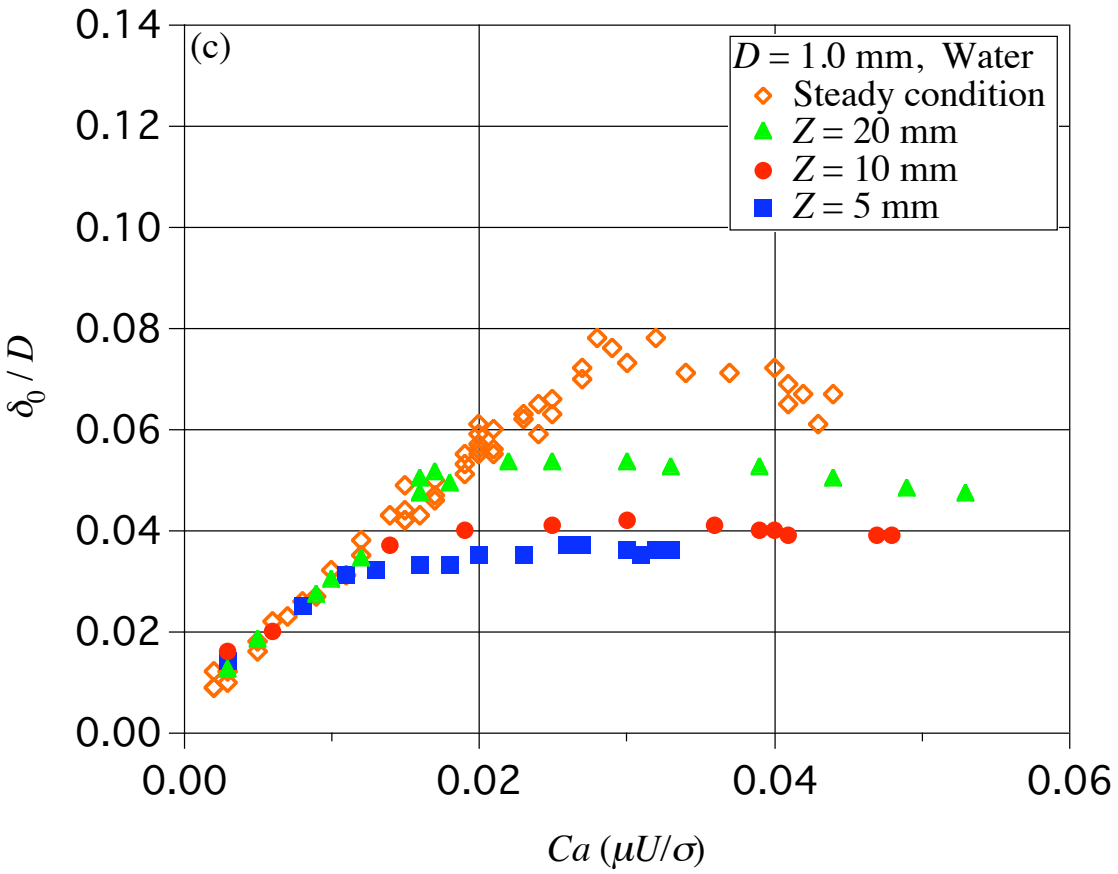

Fig. 10 Dimensionless liquid film thickness (δ_0/D) against capillary number ($Ca = \mu U/\sigma$) at different measuring points for the water/air experiment, Z = 5, 10 and 20 mm, (a) D = 0.5 mm, (b) D = 0.7 mm, (c) D = 1.0 mm.

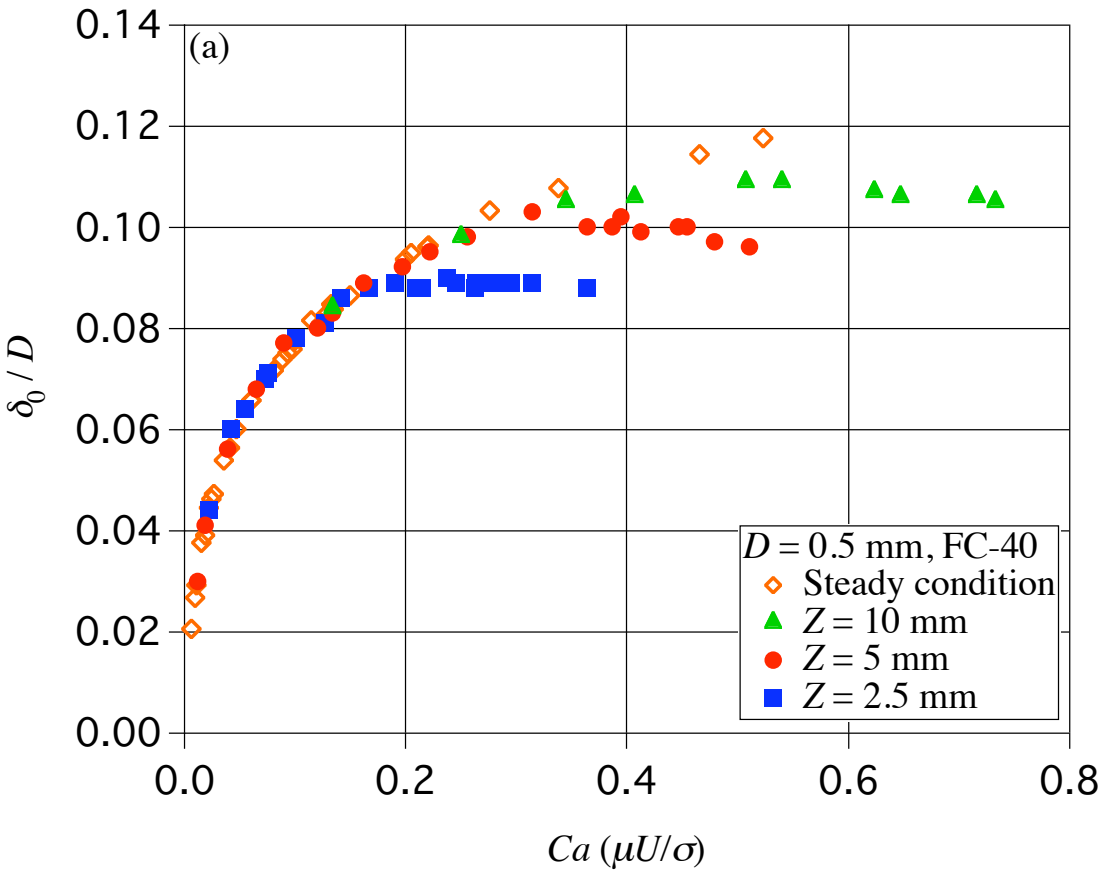
(a)
0.14
0.12
0.10
0.08
0.06
0.04
0.02
0.00
0.0
0.2
0.4
0.6
0.8
δ_0 / D
Ca ($\mu U/\sigma$)
D = 0.5 mm, FC-40
Steady condition
Z = 10 mm
Z = 5 mm
Z = 2.5 mm

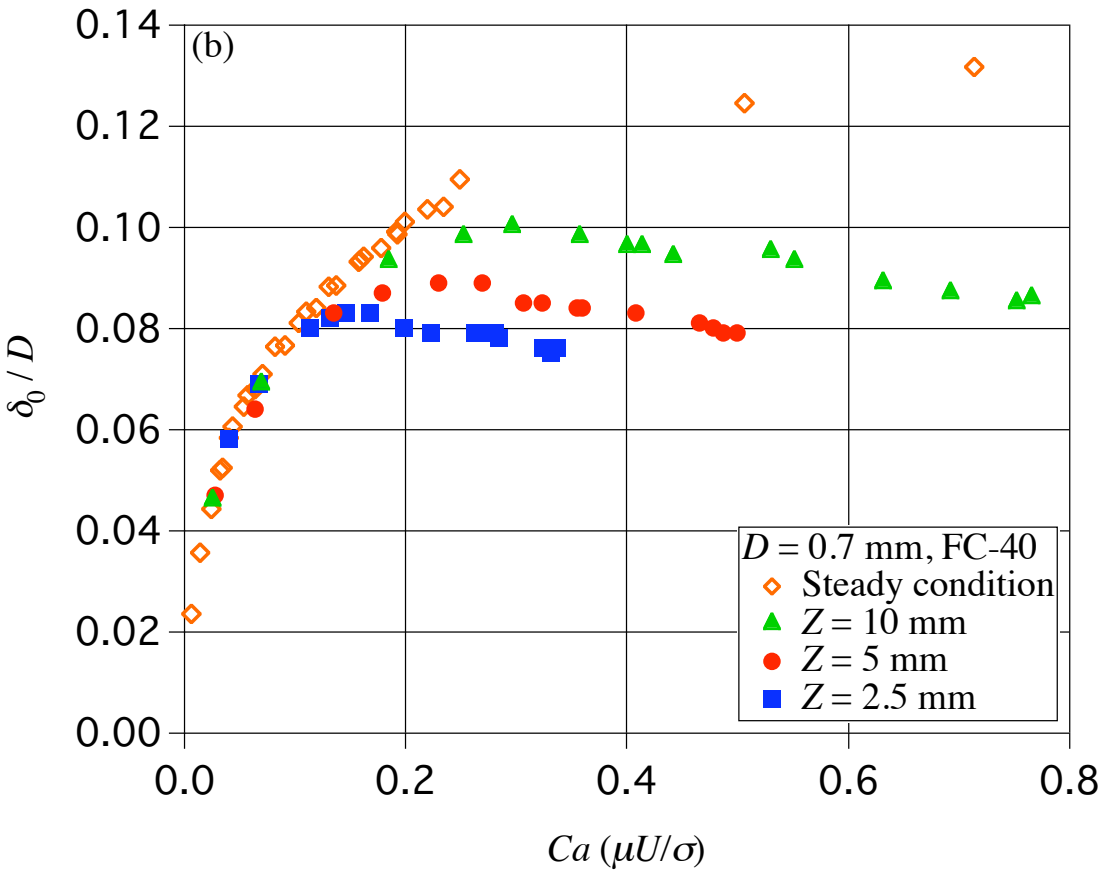
(b)
0.14
0.12
0.10
0.08
0.06
0.04
0.02
0.00
0.0
0.2
0.4
0.6
0.8
δ_0 / D
Ca ($\mu U/\sigma$)
D = 0.7 mm, FC-40
Steady condition
Z = 10 mm
Z = 5 mm
Z = 2.5 mm

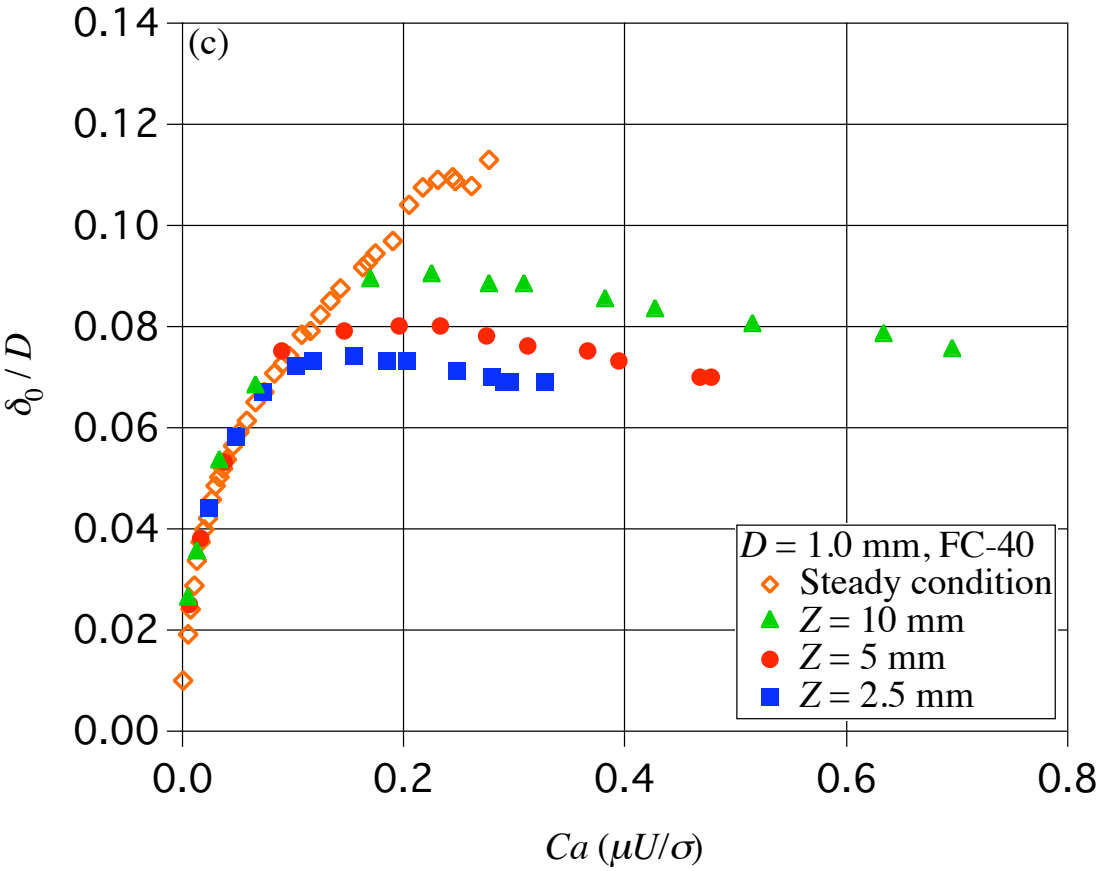

Fig. 11 Dimensionless liquid film thickness (δ_0/D) against capillary number ($Ca = \mu U/\sigma$) at different measuring points for the FC-40/air experiment, $Z = 2.5$, 5 and 10 mm, (a) $D = 0.5$ mm, (b) $D = 0.7$ mm, (c) $D = 1.0$ mm.

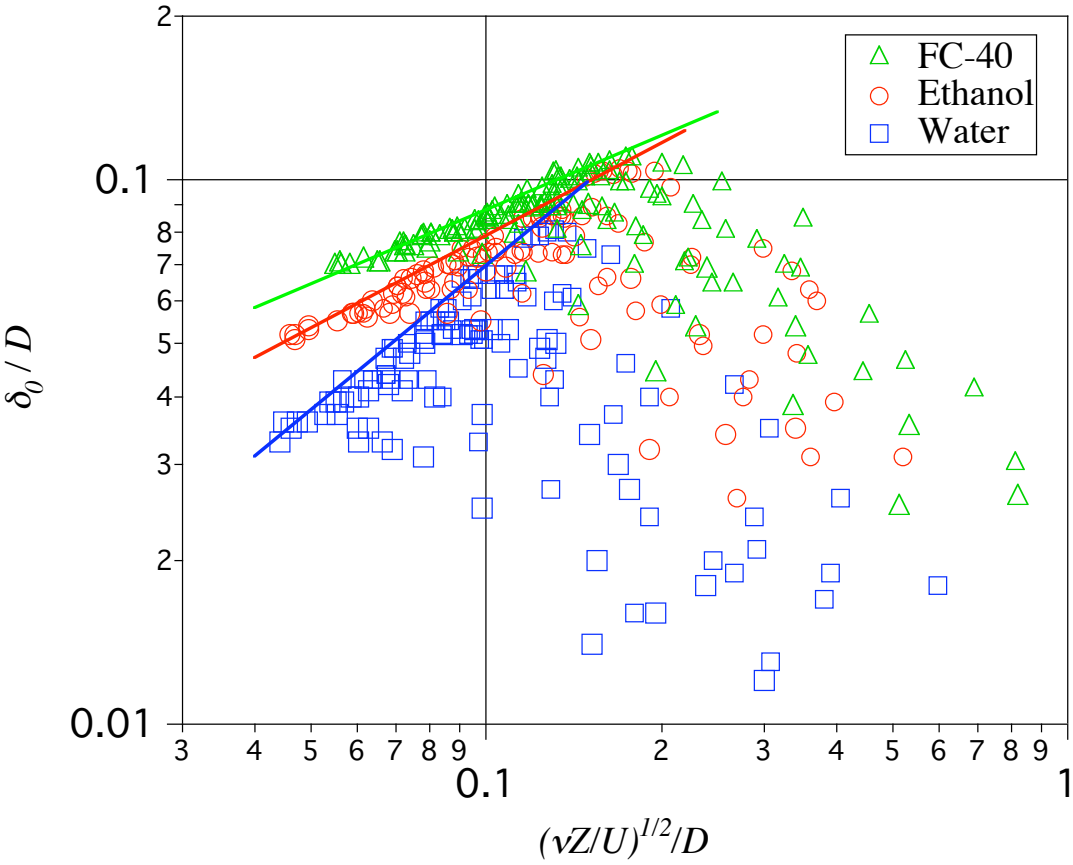

Fig. 12 Dimensionless liquid film thickness (δ_0/D) against dimensionless viscous boundary layer thickness $(\nu Z/U)^{1/2}/D$.

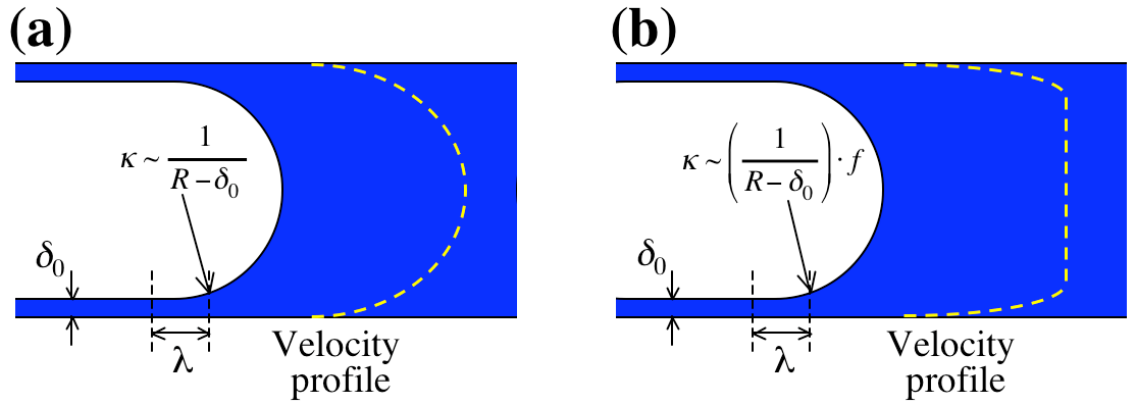

Fig. 13 Schematic diagram of velocity profiles: (a) steady condition (b) accelerated condition.

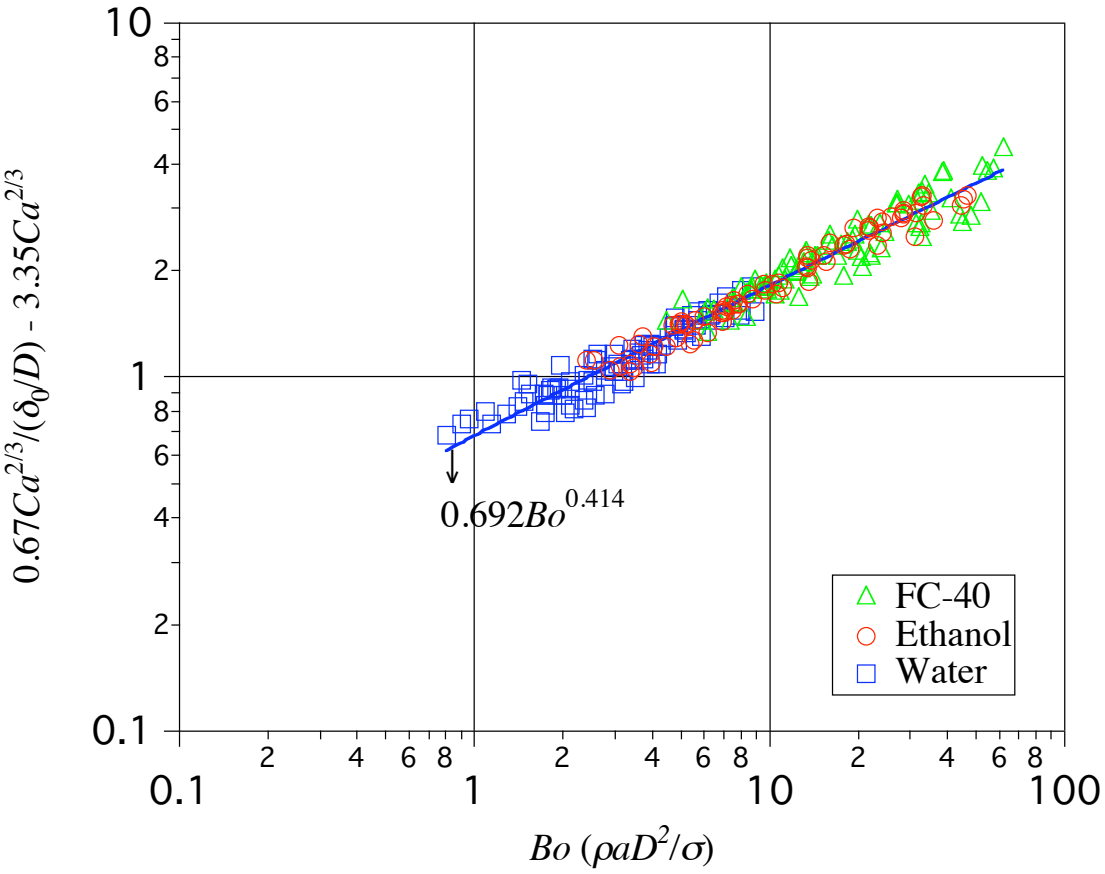

Fig. 14 R.H.S. of Eq. (16) against acceleration Bond number ($\rho aD^2/\sigma$).

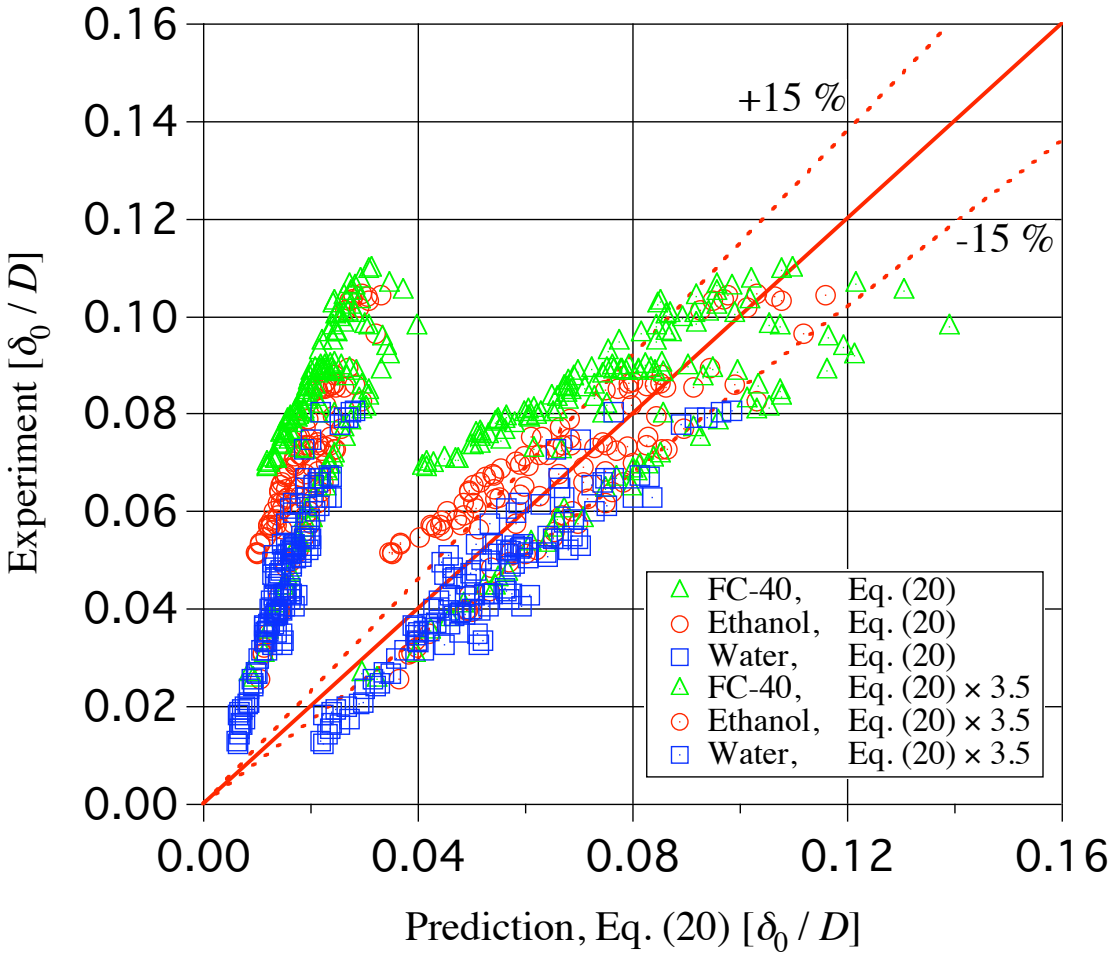

Fig. 15 Predicted liquid film thickness (δ_0/D) with the empirical correlation proposed by Moriyama and Inoue (1996), Eq. (20) against the present experimental results.

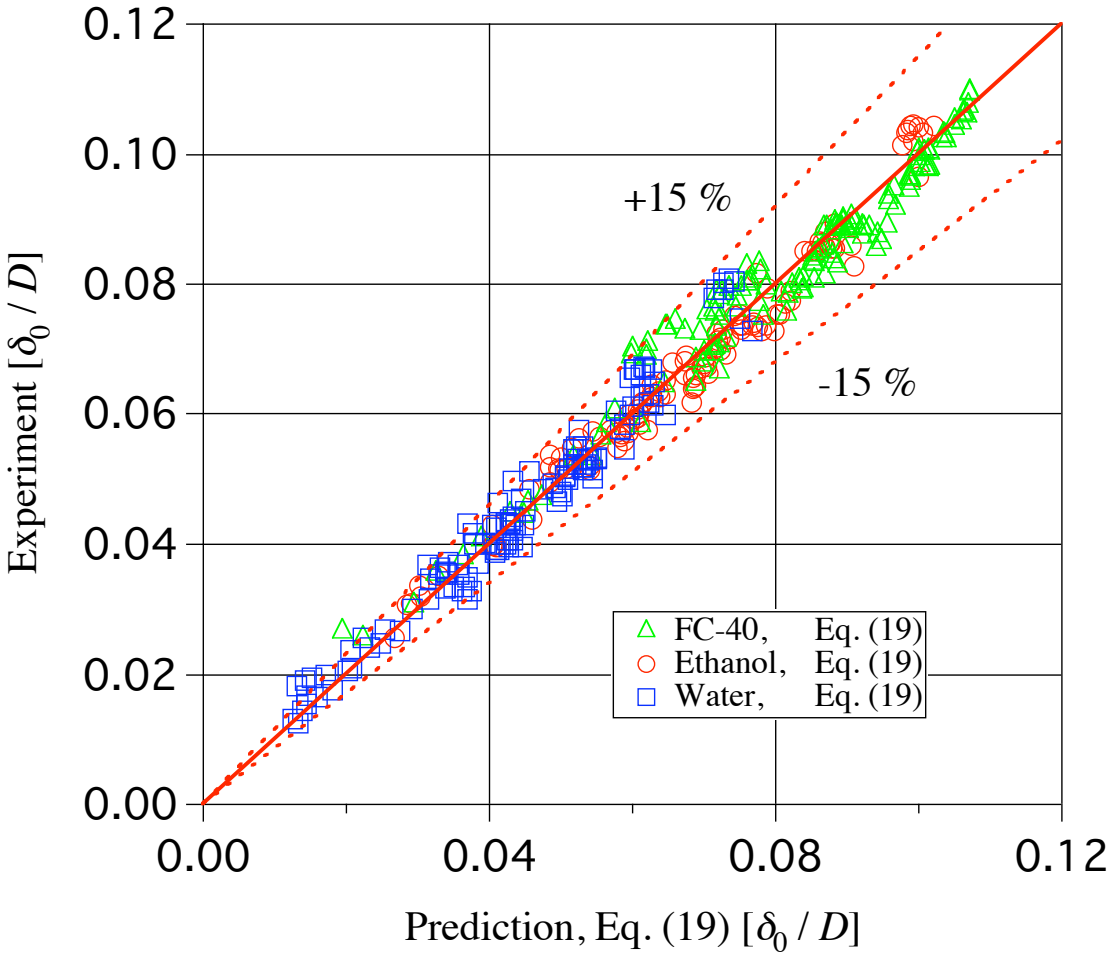

Fig. 16 Comparison between prediction, Eq. (19) and experimental results.

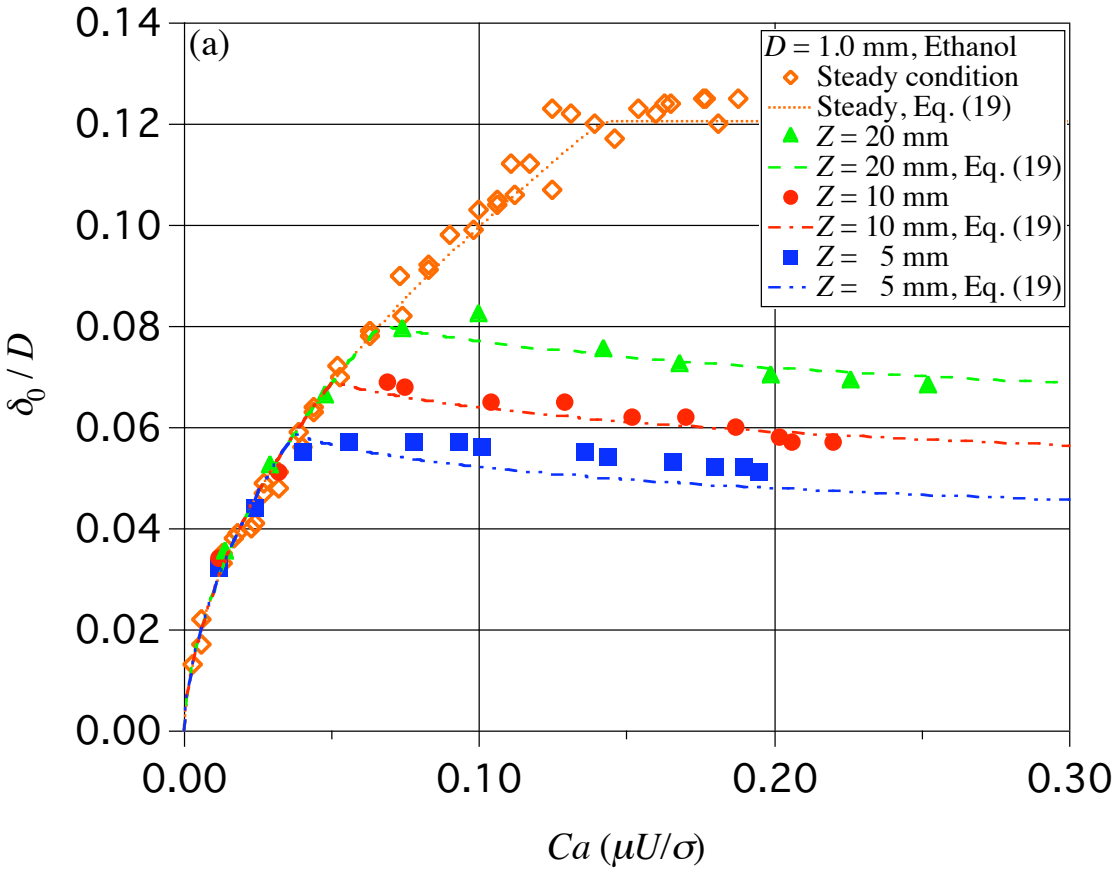
(a)
D = 1.0 mm, Ethanol
Steady condition
Steady, Eq. (19)
Z = 20 mm
Z = 20 mm, Eq. (19)
Z = 10 mm
Z = 10 mm, Eq. (19)
Z = 5 mm
Z = 5 mm, Eq. (19)
δ0 / D
0.14
0.12
0.10
0.08
0.06
0.04
0.02
0.00
0.00
0.10
0.20
0.30
Ca (μU/σ)

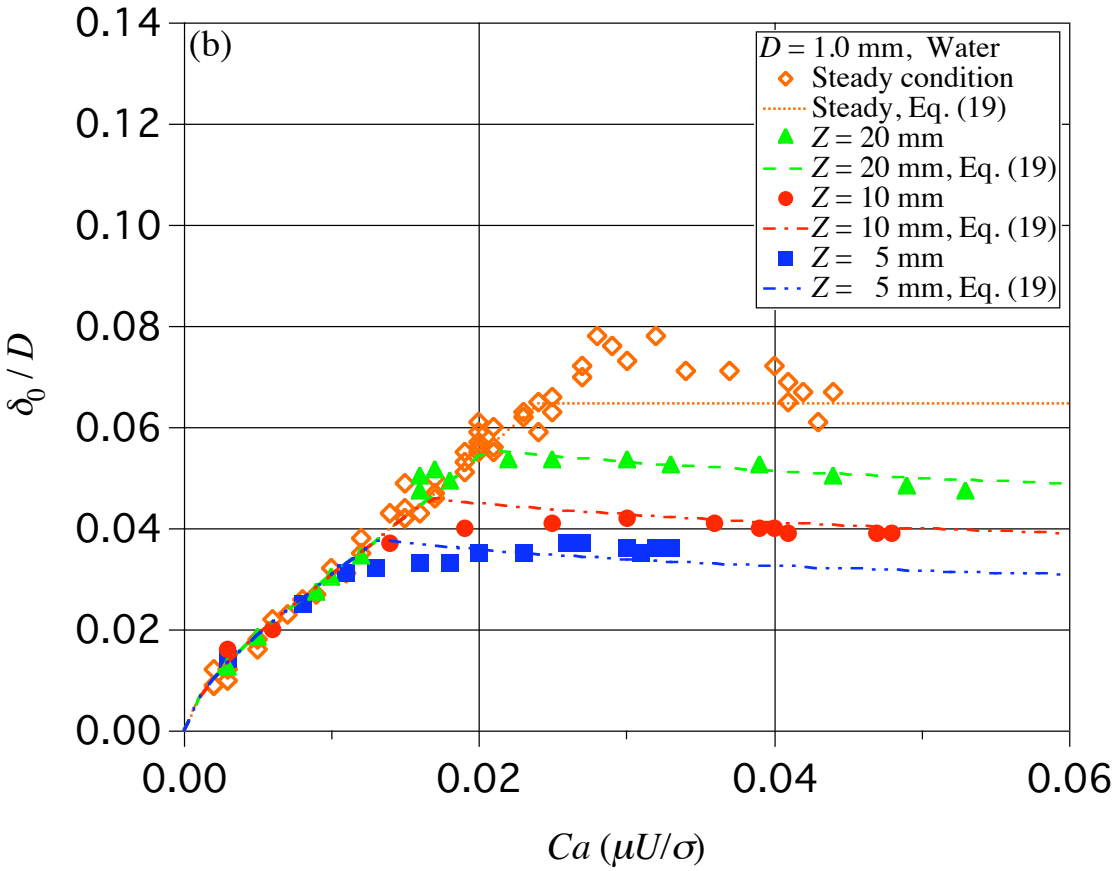
(b)
D = 1.0 mm, Water
Steady condition
Steady, Eq. (19)
Z = 20 mm
Z = 20 mm, Eq. (19)
Z = 10 mm
Z = 10 mm, Eq. (19)
Z = 5 mm
Z = 5 mm, Eq. (19)
0.14
0.12
0.10
0.08
0.06
0.04
0.02
0.00
δ0 / D
0.00
0.02
0.04
0.06
Ca (μU/σ)

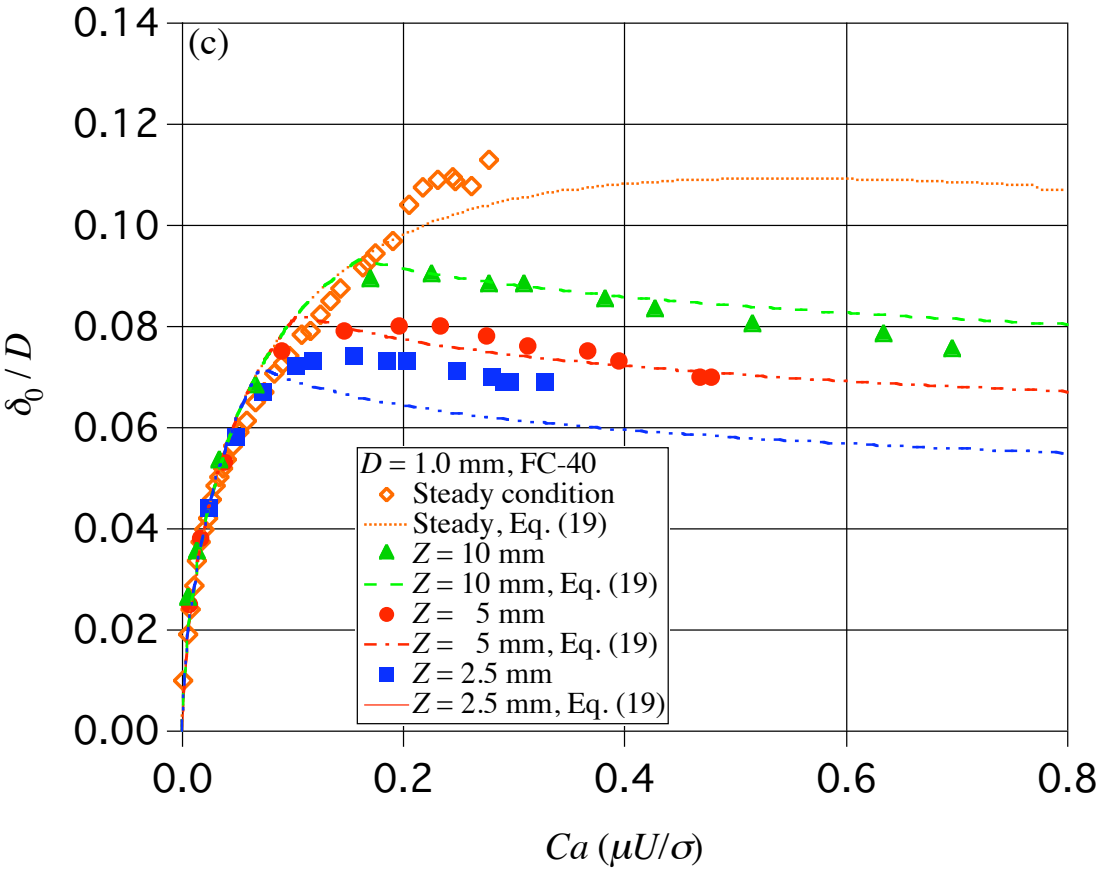

Fig. 17 Predicted liquid film thickness (δ_0/D) against capillary number ($Ca = \mu U/\sigma$), D = 1.0 mm (a) ethanol, (b) water, (c) FC-40.